Doping Concentration Influenced Pyro-Phototronic Effect in Self-Powered Photodetector Based on Ga-Incorporated ZnO Microwire/p$^+$-GaN Heterojunction

Peng Wan, Mingming Jiang, Tong Xu, Yang Liu, Xiaosheng Fang,* and Caixia Kan**

Pyro-phototronic effect, a coupling of pyroelectric and photovoltaic effect, provides an effective method to improve the performance of self-powered photodetectors (PDs). Developing high-performance PDs, the influence of pyroelectric effect on photoelectric characteristics and coupling mechanism deserves further study. Herein, a self-powered PD made of Ga-incorporated ZnO microwire (ZnO:Ga MW) and p$^+$-GaN layer is fabricated, and the performance influenced by pyro-phototronic effect is investigated systematically. Through varying Ga concentration in ZnO:Ga MWs, the pyroelectric current gradually dominates the photocurrent of PDs under ultraviolet illumination; while the photovoltaic current deteriorates rapidly. The enhanced pyroelectric responsivity can compensate the decreased photovoltaic responsivity, maintaining their high total responsivities (>5 mA W^{-1}) under self-biased conditions. Furthermore, the decay time of pyroelectric current, representing the duration of pyroelectric effect, decreases markedly from 0.313 to 0.044 s by increasing Ga concentration. Associated with theoretical analysis, incorporating Ga dopant can not only increase the rate of photogenerated temperature variation, but also narrow depletion layer at ZnO:Ga/GaN heterojunction. Besides, the temperature variation can lead to a significant reduction of decay time. These findings give a deeper insight into the influence of pyroelectric effect on photoresponse and its coupling mechanism, providing a scheme to develop high-performance self-powered PDs.

1. Introduction

Working in the absence of an external power, self-powered photodetectors (PDs) play a critical role in developing next-generation applications, such as self-sufficient micro/nanosystems, wireless multifunctional sensing, and so on.[1–4] Generally, self-powered PDs can be divided into photovoltaic detectors and thermal detectors according to their different operational mechanisms.[5] Photovoltaic detectors generate a voltage that is proportional to the incident radiation intensity due to their voltage generating characteristics.[6–8] Thermal detectors, especially pyroelectric detectors, convert photon energy to thermal energy, leading to a temperature variation in the materials and a current flow in the external circuit.[9,10] Recently, pyro-phototronic effect, combining photovoltaic effect and pyroelectric effect, has been proposed to design self-powered PDs with perfect response performances.[11,12] Despite this progress, the unambiguous working mechanism on pyroelectric–photovoltaic synergistic effect still impedes the realization of high-performance self-powered PDs. As previously reported, pyroelectric polarization charge or potential (pyropotential) is redistributed along the polar direction under time-variant temperature.[9,13–15] By introducing pyropotential, the charge transporting through the p–n/Schottky junction in self-powered PDs can be tuned, resulting in the modulation of device performance.[16–19] However, in the practical experiments and applications, the pyro-phototronic effect is sometimes absent or extremely weak in the different pyroelectric material-based p–n/Schottky junction PDs.[18,20,21] Even if the pyro-phototronic effect exists, the experimental results, such as the magnitude of the enhancement and the decay time of pyroelectric current, are quite different and fuzzy.[22,23] These phenomena indicate that some important internal physical factors that affect the pyro-phototronic effect need to be revealed further.[23,24]

Doping via incorporating electron donor or acceptor elements into the host crystal in semiconductors is a direct approach to design highly efficient electronic/optoelectronic devices. Accordingly, the electrical properties of semiconductor materials, such as conductivity and carrier concentration, can be tuned. The capability of controlling the electrical properties and the carrier transport characteristics has a significant influence on photovoltaic effect in the self-powered PDs.[25–27] In addition to tuning p–n/Schottky junction characteristics,

P. Wan, M. Jiang, T. Xu, Y. Liu, C. Kan
College of Science
MIIT Key Laboratory of Aerospace Information Materials and Physics
Key Laboratory for Intelligent Nano Materials and Devices
Nanjing University of Aeronautics and Astronautics
Nanjing 211106, P. R. China
E-mail: mmjiang@nuaa.edu.cn; cxkan@nuaa.edu.cn

X. Fang
Department of Materials Science
Fudan University
Shanghai 200433, P. R. China
E-mail: xshfang@fudan.edu.cn

The ORCID identification number(s) for the author(s) of this article can be found under https://doi.org/10.1002/adom.202101851.

DOI: 10.1002/adom.202101851

doping is demonstrated to affect photothermal heating and the thermal properties of materials.[28–31] In other words, pyroelectric effect created in materials and device's structures is significantly influenced by doping. Therefore, pyroelectric materials via doping provide a superb research platform for investigating the physical mechanisms and coupling process of photovoltaic effect and pyroelectric effect in self-powered PDs.

In this work, highly crystallized ZnO microwires (MWs) with controlled concentration of Ga dopants were synthesized using chemical vapor deposition (CVD) method. By combining p^+-GaN substrate, a single ZnO:Ga MW was utilized to construct self-powered PDs, in which the performances of device were influenced by pyro-phototronic effect. By varying the concentration of Ga dopants in the ZnO:Ga MWs, the as-constructed PDs exhibit superior detection performances. First, all the devices show enhanced responsivities which are greater than 5 mA W^{-1} under zero bias. Second, pyroelectric current gradually dominates the photocurrent, companied by the significant reduction of the photovoltaic current simultaneously. As the concentration of Ga dopants exceeds a certain value, the photocurrent is mainly dominated by the pyroelectric current. Third, the decay time of pyroelectric current has been greatly reduced from 0.313 to 0.044 s. It is proposed that the significantly optimized performances are ascribed to the pyro-phototronic effect. Further, to study the coupling mechanism between pyroelectric effect and photovoltaic effect, the doping concentration will remarkably affect interface states of the as-formed n-ZnO:Ga MW/p^+-GaN heterojunction. Besides, the effect of photoinduced heating on the device performance was studied. The results illustrated that increasing the concentration of Ga dopants can increase the rate of temperature variation, which is responsible for the enhancement of pyroelectric current. These findings not only help us to further clarify the coupling of pyroelectric and photovoltaic synergistic effect modulated by the doping concentration, but also can afford great significance to develop high-performance self-powered detectors.

2. Results and Discussions

The self-powered ultraviolet PD consisting of single ZnO MW and p^+-GaN is schematically shown in **Figure 1**a. Details about the fabrication process are available in the Experimental Section. The current–voltage (*I–V*) curves of the fabricated ZnO MW/p^+-GaN heterojunction device under dark and UV illumination (λ= 370 nm, 0.5 mW cm^{-2}) are plotted in Figure 1b. The ZnO MW/p^+-GaN PD shows a photovoltaic effect under UV illumination and can work without external bias voltage. Due to the ohmic contact between metal electrode and semiconductor (Figure S1, Supporting Information), the rectifying behavior and photovoltaic effect are originated from the p–n junction between the ZnO and the GaN.[17,32] The energy band

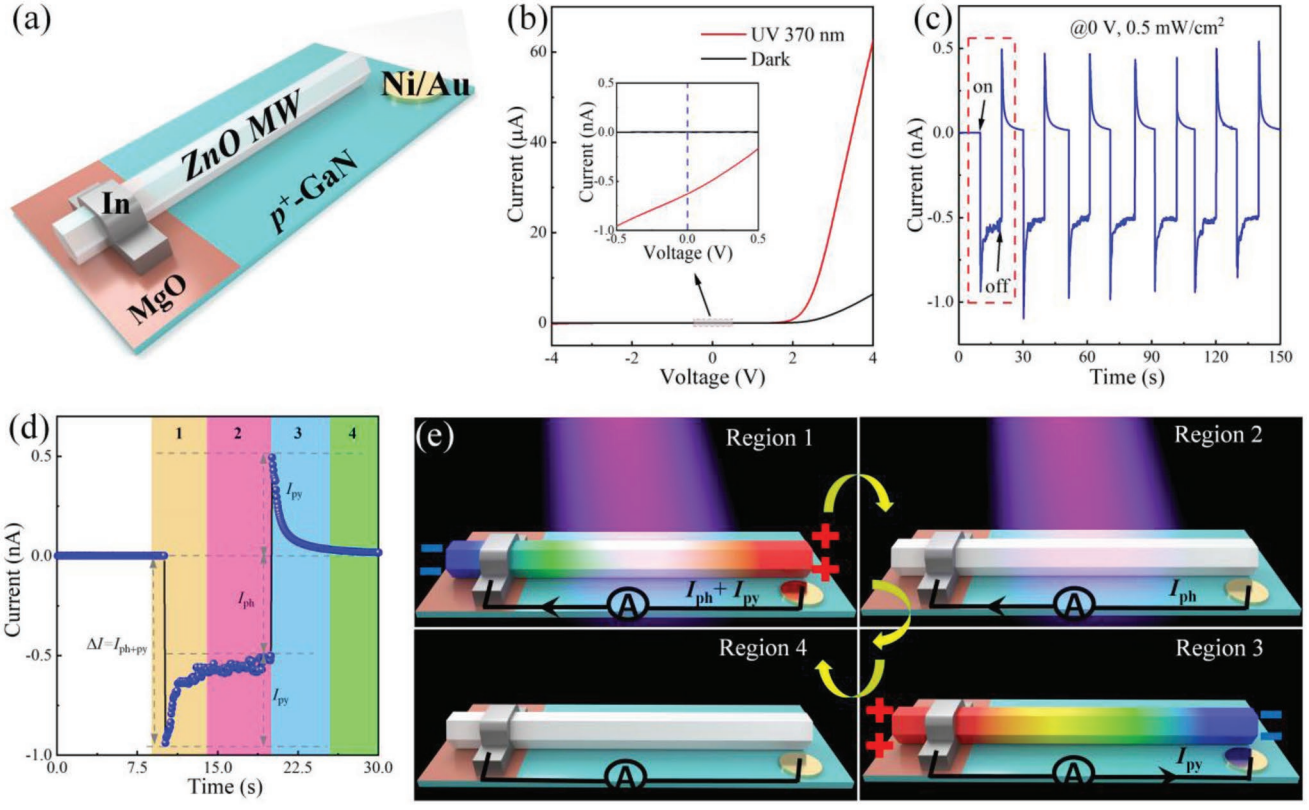

Figure 1. a) Schematic illustration of the self-powered ZnO MW/p^+-GaN PD. b) *I–V* curves of the ZnO MW/p^+-GaN PD under dark and UV illumination. The inset is the enlarged *I–V* curves under low applied bias. c) *I–t* response of the ZnO MW/p^+-GaN PD in the absence of external power, where UV illumination (λ= 370 nm, 0.5 mW cm^{-2}) is switched on and off periodically. d) Amplification of one period of *I–t* curve in the red dashed box in (c). e) Schematic illustration of photoelectric response mechanism of the ZnO MW/p^+-GaN PD corresponding to the four regions shown in (d).

alignment of the as-prepared PD with the corresponding band positions is shown in Figure S2 (Supporting Information). Under UV illumination, the photoinduced electrons move from the ZnO MW to the In cathode while the holes transfer to the Ni/Au anode through the p^+-GaN due to built-in electric field, leading to the formation of photovoltaic current.[33,34] Figure 1c shows the cyclic current-time (*I–t*) curves of the ZnO MW/p^+-GaN PD in the absence of external power, in which the UV light is switched on and off periodically. It is found that the response current keeps well-reproducible in the transition between on and off of UV light. Once the UV light is switched on, a sharp increase in the response current appears and subsequently the current decays to a steady state. Upon switching off the UV light, the current quickly changes in the negative direction and then reduces to zero. The dynamic current behavior of *I–t* curves was studied, and could be assigned to pyro-phototronic effect,[11] or alternating current photovoltaic effect.[35] By comparison, the alternating current photovoltaic effect makes the devices possessing ultrafast response time (lower than 20 μs), which is originated from a relative shift and realignment between the quasi-Fermi levels under the nonequilibrium conditions.[35] Due to the long duration of response (about several milliseconds) in ZnO MW/p^+-GaN PD, the observed current behavior can be attributed to pyro-phototronic effect (Some discussion in detail is available in Note S3 in the Supporting Information). In addition, the AC photovoltaic effect is truly universal since it exists for various types of junctions.[35] Nevertheless, the AC photovoltaic effect cannot be detected in the as-constructed photodetection devices. The main reason is attributed to test equipment with low sampling rate (10^2–10^3 Hz per second), which cannot meet the requirement for obtaining AC photovoltaic signal (10^5–10^6 Hz per second).

One period of *I–t* curve is amplified in Figure 1d, where the current behavior is divided into four regions (region 1, region 2, region 3, and region 4). In region 1, when the UV light is switched on, light-induced transient increase of temperature introduces pyroelectric charges (potential), which reduces the potential barrier at the heterojunction interface and accelerates light-induced charge separation and transport. A sharp peak occurs in photocurrent labeled as I_{ph+py}. After a certain period of time, the temperature of ZnO MW no longer changes and the pyroelectric effect vanishes. The response current in region 2 decays to I_{ph}. The I_{ph} can be assigned to photovoltaic effect in the PD.[19] Once the UV light is off, the sudden decrease in temperature will cause the reverse distribution of pyroelectric charge across ZnO MW (See Figure 1e) and a reverse pyroelectric current in region 3. Finally, the response current approaches dark current (I_d) in region 4 because the temperature tends to be stable without the illumination of UV light. Furthermore, the ZnO MW/p^+-GaN PDs are thoroughly probed based on the effect of externally applied bias, background temperature and near-infrared illumination (Figures S3–S5, Supporting Information), which is consistent with the dynamic current behavior induced by pyro-phototronic effect.[18,22]

As previously reported, the pyro-phototronic effect is ascribed to pyroelectric semiconductors as well as the constructed p–n/Schottky junction.[18,19,22] To fabricate self-powered PDs with the performance enhanced by pyro-phototronic effect, doping is expected to tune the junction and pyroelectric charge, further exploring the formation mechanism of the pyro-phototronic effect.[28] The influence of the Ga doping concentration on the morphological, structural and optical properties of ZnO MW is explored systematically. SEM images of the MWs with different Ga doping concentrations are shown in Figure S6 (Supporting Information). All the samples exhibit smooth and uniform surfaces with hexagonal cross section, demonstrating that the incorporation of Ga element causes little damage to the morphologies of the MWs. As illustrated in the EDS Mapping results, Ga element is evenly distributed in the MWs (Figure S7, Supporting Information). Increasing Ga_2O_3 powder in the precursors can be used to increase the Ga doping concentration in the as-synthesized ZnO:Ga MWs.[35] The XRD patterns of the ZnO MWs with different Ga doping concentrations are shown in **Figure 2**a. The diffraction peaks show that all the samples have typical single-phase wurtzite-type structure without any other phases. This result suggests that the Ga dopants have been incorporated into the ZnO lattice.[36] In addition, the variation of relatively intense and line width of diffraction peaks also indicates that the substitution of Ga for Zn can be achieved.[17,26]

The optical properties of as-prepared ZnO:Ga MWs with different Ga-doping concentrations are characterized. The samples show negligible absorption over visible band, suggesting that these as-developed PDs can operate in the UV spectral range (Figure 2b).[37] The cutoff edge shifts toward shorter wavelength with the increase of the Ga doping concentration (inset in Figure 2b). According to the Tauc's formula,[17] the optical bandgap (E_g) is calculated in Figure S8 (Supporting Information). The incorporation of Ga element in ZnO MW can contribute to the broadening of the optical bandgap.[20] It should be noted that, the specific absorption values may be not accurate due to the limitation of the size and special shape of the hexagonal wires. Thus, the absorption results of different samples cannot be compared with each other directly. In fact, the undoped or doped ZnO materials possess large ultraviolet (UV) absorption coefficient (10^4–10^5 cm^{-1}).[38] The influence of doping concentrations on absorption in ultraviolet band can be negligible. Further to characterize the influence of Ga doping concentration on the optical properties of individual ZnO:Ga MWs, room-temperature photoluminescence (PL) measurement was carried out. As shown in Figure 2c, the intense emission peak (≈380 nm) is observed in the samples, which can be attributed to the typical near-band-edge emission of ZnO.[39] Additionally, broadband visible emission associated with deep level is also acquired in the undoped ZnO MW. The deep-level dependent emission is originated from the transitions between some intrinsic defects such as V_O and Zn_i.[40] By introducing Ga dopants, the visible emission observed in undoped ZnO MWs is significantly reduced, indicating that the Ga-incorporation via moderate doping concentration improves crystallization quality and optical properties of the as-grown samples.[41,42]

Possessing non-centrosymmetric crystal structure and specific polar axis along the direction of spontaneous polarization, individual ZnO:Ga MW can work as a common pyroelectric semiconductor material.[43] Crystal symmetry of the MWs was investigated by a non-destructive and sensitive second-harmonic generation (SHG) method, which is only allowed in the materials lacking inversion symmetry (Schematic illustration of the setup for the SHG measurement is shown in the inset of

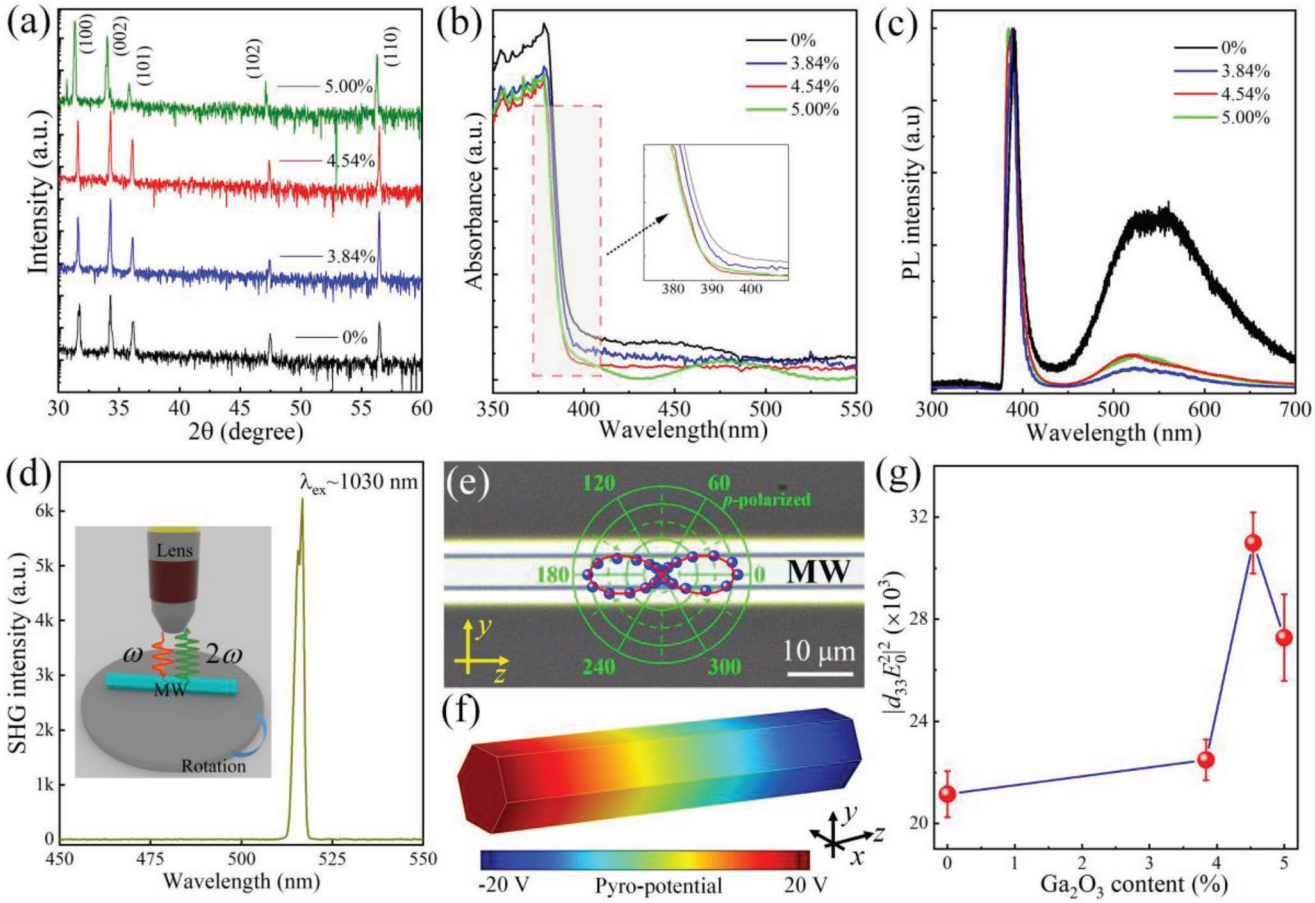

Figure 2. a) XRD patterns of MWs with different Ga doping concentrations. b) Absorption spectra of MWs with different Ga doping concentrations. c) PL spectra of individual ZnO MWs with the Ga doping concentrations. d) SHG spectrum of a single ZnO MW. The inset is a schematic illustration of the setup for the SHG measurement. e) Typical optical image of single ZnO MW along growth-direction (z-direction). The inset is polar plot of the SHG intensity of the ZnO MW as a function of rotation angle θ. f) The simulated distribution of pyropotential along the ZnO MW. g) The SHG intensity along the growth direction of ZnO:Ga MW ($|d_{33}E_0^2|^2$) with the weight ratio of Ga_2O_3 in the source materials ranging from 0% to 5.00%.

Figure 2d).[44] Under the excitation of 1030 nm laser, an intense SHG peak (≈515 nm) can be observed from the undoped ZnO MW, which is exactly equal to the half of the excitation wavelength (See Figure 2d). The second-order nonlinear process indicates that the as-synthesized MW is a non-centrosymmetric crystal structure.[45] The polarized SHG measurement with a polarization parallel and perpendicular to the polarized excitation laser was carried out to study further the symmetry of MW (Note S9, Supporting Information). The clear twofold polarimetric pattern (*p*-polarized) in Figure 2e reveals that polar *c*-axis is parallel to the MW's long-axis and two hexagon sections are polar surfaces.[46,47] Thus, the polarization-induced positive and negative electric charge will assemble at the both ends of single MW.[18] Generally, the generated pyroelectric current i is expressed as[23]

$$i = pA\frac{\mathrm{d}T}{\mathrm{d}t} \tag{1}$$

where p, A, and $\mathrm{d}T/\mathrm{d}t$ are the pyroelectric coefficient (≈1.2 nC cm^{-2} K for ZnO),[10] the sensing area and the rate of temperature change, respectively. From Equation (1), pyroelectric behavior is originated from the polarization level, which is dependent on temperature variation rate $\mathrm{d}T/\mathrm{d}t$. Furthermore, the pyropotential U built in the MW can be described as[48]

$$U = \frac{p\Delta T l}{\varepsilon_{33}\varepsilon_0} \tag{2}$$

where ΔT, l, ε_{33}, and ε_0 are the temperature change, the size of MW, the relative permittivity of ZnO in the polarization direction (≈8) and the permittivity of vacuum, respectively. Combined with Equation (2) and finite element method, the calculated pyropotential distribution of MW is shown in Figure 2f, in which the ΔT and l are chosen as 5 °C and 50 μm, respectively. It is demonstrated that there are inverse pyropotential drops along the MW under the temperature fluctuations, which will play a key role in the modulation on the device performances of a single MW-based self-powered PDs.[49] The influence of the Ga doping concentration on the polarimetric SHG intensity (*p*-polarized and *s*-polarized) of MW was studied. The incorporation of Ga element has little impacts on the polarization direction along the MW (*p*-polarized) in Figure S10 (Supporting Information). In addition, the polarimetric patterns

(*s*-polarized) of MW with larger Ga doping concentrations are different from that of MW with lower Ga doping concentrations due to the twin boundaries and the 3*m* symmetry induced by the polar strength of Zn—O bonding.[50] The SHG signal polarized along the *c*-axis in MW is mainly originated from its second-order nonlinear susceptibility component d_{33}. As shown in Figure 2g, the SHG intensity along the direction of MW ($|d_{33}E_0^2|^2$) improves with the incorporation of Ga element, revealing that the formation of quasi-interfaces in MWs contributes to these symmetry breaking interfaces.[44]

The dynamic photoelectric response features of as-constructed n-ZnO:Ga MW/p^+-GaN self-powered PDs are carefully investigated under the illuminations of 370 nm. In the fabricated PDs, individual ZnO:Ga MWs were selected from the as-synthesized samples by varying the weight ratio of Ga_2O_3 in the source materials, such as 0%, 3.84%, 4.54%, and 5%, respectively. By increasing the intensity of the illuminated light, typical *I*–*t* curves are displayed in **Figure 3**. An enlarged view of one period of *I*–*t* curve is shown in the right of Figure 3. Clear photovoltaic and pyroelectric current are observed from the PDs, demonstrating that the built-in potential at n-ZnO:Ga/p^+-GaN interface can be formed, and the corresponding pyro-phototronic effect can also be observed.

The extracted photovoltaic currents I_{ph} are depicted in **Figure 4**a, respectively. A clear enhancement in the I_{ph} with an increase of incident light density is obtained. And the enhancement is assigned to the fact that photogenerated carriers are positively correlated to the photon flux.[24] Simultaneously, the larger incident light intensity can causes the higher temperature in the as-constructed PDs, further contributing to the increase of pyroelectric current I_{py} (See Figure 4b). For the undoped ZnO MW-based PD, the collected photocurrent is mainly dominated by the photovoltaic current. The I_{ph} and I_{py} are estimated to −2.5 and −1.0 nA, respectively (See Figure 4c, the light intensity ≈ 5.00 mW cm^{-2}). For the ZnO:Ga MW (3.84%), the photovoltaic current extracted from the as-constructed PD is significantly increased to −5.2 nA. The increased photovoltaic current is attributed to the reduced surface defects and the increased carrier transport properties of the ZnO:Ga MW induced by the appropriate concentration of Ga dopant.[27,51,52] Further increasing the concentration of Ga dopant in ZnO:Ga MWs, a sharp reduce of the photovoltaic

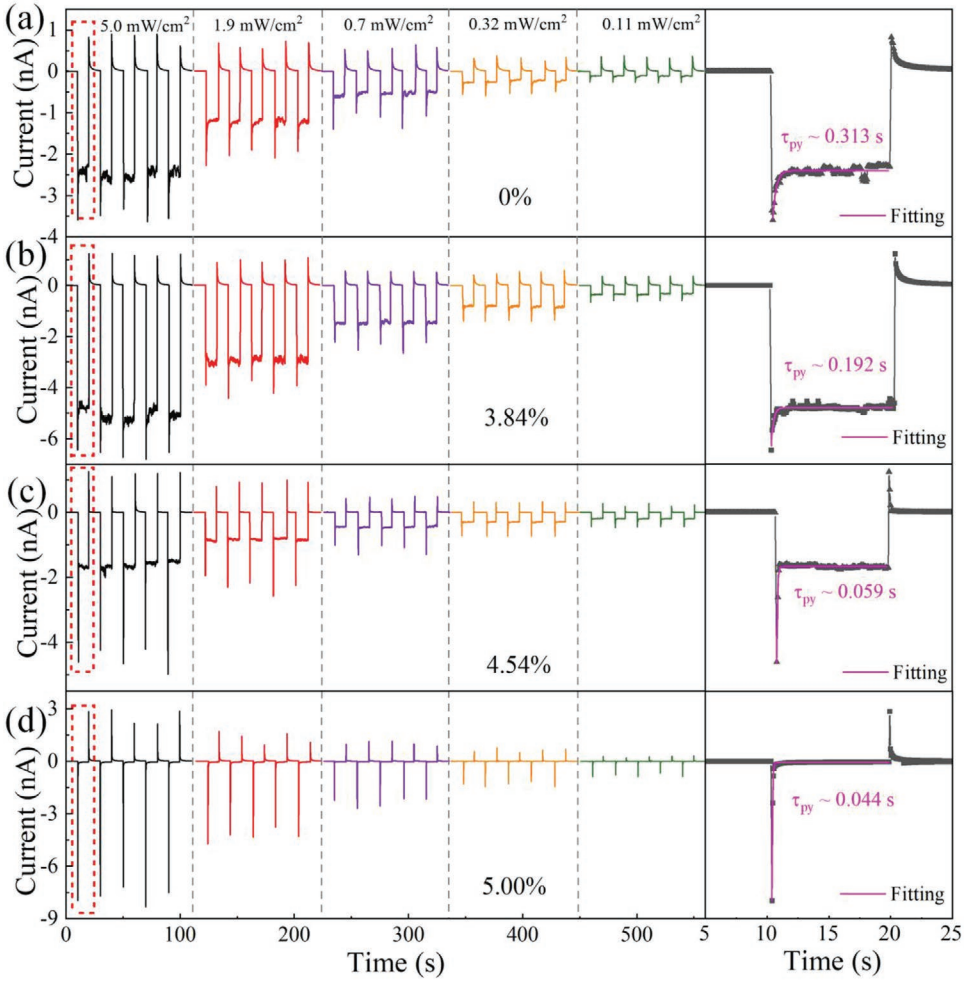

Figure 3. *I*–*t* curves of MW/p^+-GaN PDs under UV 370 nm illumination with different light intensities, in which the MWs contain different Ga doping concentration: a) 0%, b) 3.84%, c) 4.54%, d) 5.00%. The right enlarged view of the single cycle *I*–*t* curve showing four distinct regions of the photovoltaic current and pyroelectric current. The pink line is the fitting curve of the decay time of pyroelectric current (τ_{py}).

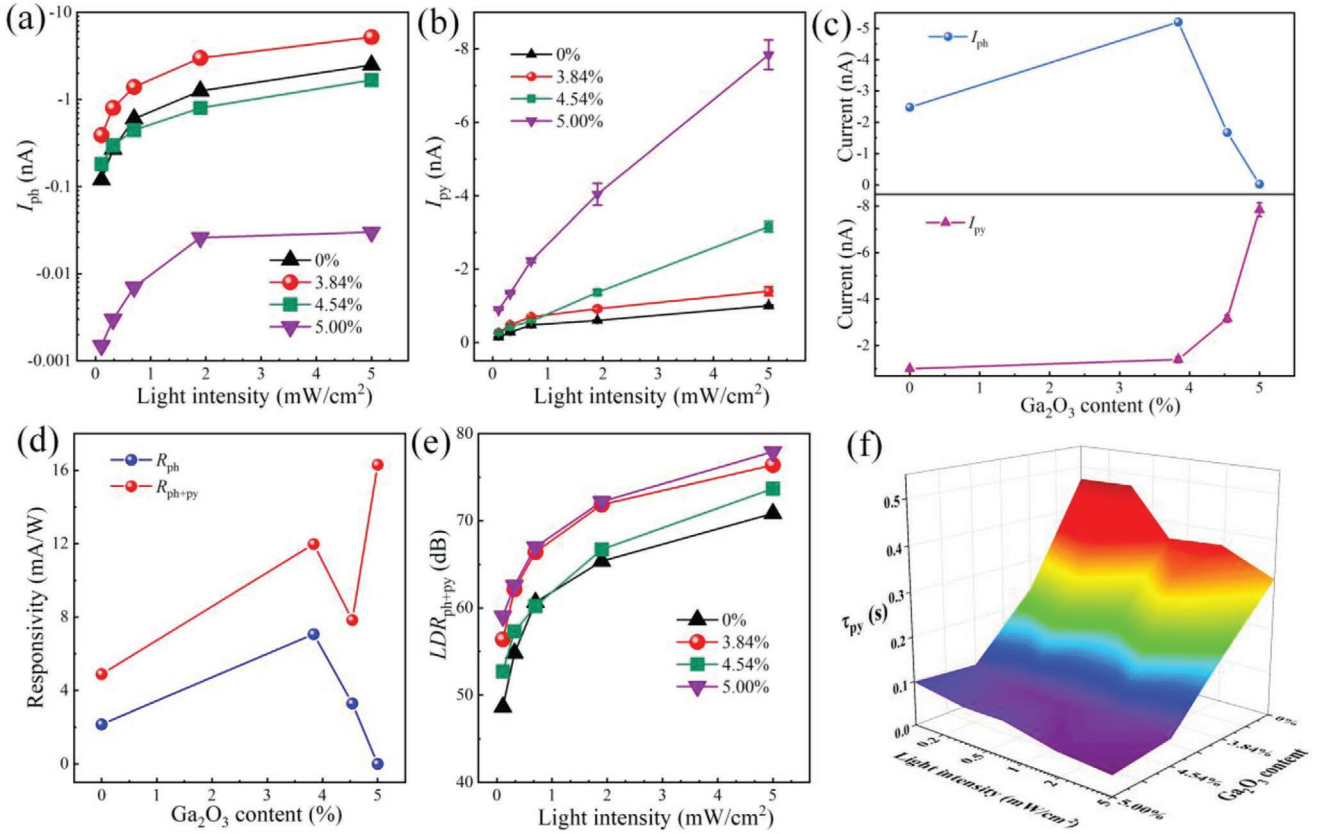

Figure 4. a) Photocurrent (I_{ph}) and b) pyroelectric current (I_{py}) of the PDs fabricated by MWs with different Ga doping concentrations under the different UV illumination intensities. c) The corresponding photocurrent (I_{ph}) and pyroelectric current (I_{py}) of the PDs under UV illumination (5.00 mW cm^{-2}). d) The corresponding photovoltaic responsivity response (R_{ph}) and the responsivity (R_{ph+py}) of the PDs under UV illumination (0.11 mW cm^{-2}). e) The corresponding linear dynamic range (LDR_{ph+py}) of the PDs under different UV intensities. f) 3D mapping of decay time (τ_{py}) of the PDs.

current appears; and the pyroelectric current exhibits an observable increase. Under different intensities of UV illumination, this trend is consistent (Figure S11, Supporting Information). The decreased photovoltaic current can be attributed to the concentration of Ga dopant in the ZnO:Ga MWs. With increase of Ga_2O_3 content in the source materials, tunable n-type conduction and their corresponding carrier concentration are achieved (Note S11 and Table S1, Supporting Information). The relatively high carrier concentration in ZnO:Ga MWs can narrow the depletion layer in the as-constructed n-ZnO:Ga/p$^+$-GaN heterojunction devices ranging from 730 to 23 nm (Note S12 and Table S2, Supporting Information). The sharply narrowed depletion layer gives rise to dramatic deterioration of the photovoltaic current, further reducing photovoltaic sensitivity.[53,54] It is worth noting that high carrier concentration can cause screening effect and partially reduce the polarization potential in ZnO materials.[55] The calculated carrier concentration is far away from Mott concentration ($\approx 4.2 \times 10^{18}$ cm^{-3}) even for ZnO:Ga MW (5.00%). The influence of screening effect on pyroelectric polarization in the ZnO:Ga MW can be negligible.[56] The reason for the increased pyroelectric current will be discussed later.

The total responsivity (R_{ph+py}) and photovoltaic responsivity (R_{ph}) of the PDs fabricated by ZnO:Ga MWs with different Ga concentrations under UV illumination (0.11 mW cm^{-2}) are shown in Figure 4d. Detailed calculation is available in Note S13 (Supporting information). The evaluated R_{ph+py} are always greater than R_{ph} for all the as-constructed PDs. Besides, the total detectivity (D^*_{ph+py}) is always larger than photovoltaic detectivity (D^*_{ph}) (Figure S12, Supporting Information). These results reveal that the significant enhancement in responsivity and detectivity of PDs can be achieved by introducing pyro-phototronic effect. The total R_{ph+py} maintains a relatively high value for all the as-constructed n-ZnO:Ga MW/p$^+$-GaN PDs (>5 mA W^{-1}), in which the major contribution is pyroelectric responsivity (R_{py}). Based on the enhanced ratios of R (Figure S13, Supporting Information), pyro-phototronic effect can be used to compensate the rapidly decreased photovoltaic responsivity in heavily doped ZnO:Ga MW-based PDs. As shown in Figure 4e, the total linear dynamic range (LDR_{ph+py}) is improved by incorporation of Ga dopant. The maximum LDR_{ph+py} is estimated to be ≈75 dB, which is larger than that of commercial InGaAs-based PDs (≈66 dB).[32]

The decay time of pyroelectric current depicts the duration of pyroelectric effect on self-powered PDs. 3D mapping of decay time of the PDs is shown in Figure 4f. With an increase of the Ga doping concentration, the τ_{py} of the as-constructed PDs decreases gradually. In addition, the τ_{py} is relatively insensitive

to the different intensities of UV illumination. Interestingly, τ_{py} is intensively correlated to the heterojunction materials instead of the background temperature (Figures S14 and S15, Supporting Information).

In order to explore the reason for the enhanced pyroelectric current and the decreased decay time τ_{py}, the influence of Ga doping concentrations on light-induced temperature variation is analyzed. First, the key parameters affecting temperature variation are derived. The temperature difference ΔT between the material and the surroundings can be obtained from heat balance equation[23]

$$\eta W(t) = H\frac{\mathrm{d}\Delta T}{\mathrm{d}t} + G_T \Delta T \tag{3}$$

where η, H and G_T are photothermal conversion efficiency, the thermal capacity and the thermal conductance to the surroundings, respectively. The power of incident radiation $W(t)$ is defined as $W_0 e^{i\omega t}$, where W_0 is the light source power and ω is the chopping frequency. The solution of Equation (3) is

$$\Delta T = -\frac{\eta W_0 e^{-t/\tau}}{G_T + i\omega H} + \frac{\eta W_0 e^{i\omega t}}{G_T + i\omega H} \tag{4}$$

where τrepresents the thermal time constant ($\tau = H/G_T$). If $\omega \to 0$, the ΔT and the temperature variation rate $\mathrm{d}T/\mathrm{d}t$ can be written as

$$\Delta T = \frac{\eta W_0}{G_T}\left(1 - e^{-t/\tau}\right) \tag{5}$$

$$\mathrm{d}T/\mathrm{d}t = \frac{\eta W_0}{H} e^{-t/\tau} \tag{6}$$

which describes the transient temperature difference and temperature variation rate of the material once the light is switched on.

Then, thermal imaging of MWs was measured under the UV illumination (λ = 370 nm, 10.0 mW cm^{-2}). The testing method is available in Note 16 (Supporting Information). To make sure that the photoinduced heat comes from the samples, thermal effect of glass and background is excluded in Figure S17 (Supporting Information). The thermal imaging demonstrates that the as-grown ZnO:Ga MWs with different Ga doping concentrations can absorb UV light, and then produce heat. As shown in **Figure 5**a–d, the heat generated in the ZnO:Ga MWs increases with increasing the concentration of Ga dopant. The highest temperature (27.9 °C) is observed from the ZnO:Ga MWs (5.00%), as illustrated in Figure 5e. Combined with Equation (5), it can be found that the heavily doped MWs exhibit higher photothermal conversion efficiencies η in the case of the same thermal conductivity. The photothermal conversion efficiency of as-grown ZnO:Ga MWs is quite difficult to measure directly; while the electrical conductivity (σ) of individual ZnO:Ga MWs is positively relative to the concentration of Ga dopant. According to electromagnetic heating effect, photothermal effect yielded in ZnO:Ga MWs could be evaluated by means of the electrical conductivity.[57] The I–V curves of individual ZnO:Ga MWs with different Ga-doping concentration are plotted in Figure 5f. Electrical measurements of individual ZnO:Ga MWs show that increasing Ga_2O_3 in the source materials can indeed increase electrical conductivity (See Figure 5g).

Based on the above theoretical analysis and experimental results, the influence of electrical conductivity on the temperature of ZnO:Ga MWs was simulated using finite element method (Detailed information can be referred to Note S17 in the Supporting information). Figure 5h shows the distribution of simulated temperature of a single undoped ZnO MW. Higher temperature is observed in the ZnO:Ga MWs with larger σ (Figure S18, Supporting Information). The temperature as a function of time is shown in Figure 5i. Upon UV illumination, the temperature rises quickly and then levels up to a stable value, which is consistent with Equation (5). The temperature variation (ΔT) of the ZnO MW is positively influenced by σ, which is in accord with experimental results (Figure 5e,g). In addition, ZnO:Ga MWs with high σ exhibit higher peak value and faster decay speed of $\mathrm{d}T/\mathrm{d}t$, as shown in Figure 5j. It is demonstrated that the ZnO MW with higher doping concentrations can give rise to faster temperature variation under UV illumination.

To describe the pyroelectric current behavior further, combined with Equations (1) and (6), the current i can be written as

$$i = pA\frac{\eta W_0}{H} e^{-t/\tau} \tag{7}$$

which describes instantaneous current signal of the pyroelectric material once the light is switched on. Based on Equation (7), the reason for the enhanced pyroelectric current and faster decay speed of pyroelectric current, which are induced by Ga doping concentrations, can be summarized. The ZnO:Ga MWs with high doping concentrations have larger electric conductivity σ, introducing high photothermal conversion η under UV illumination. The high photothermal conversion further leads to high rate of temperature variation $\mathrm{d}T/\mathrm{d}t$. Finally, the large pyroelectric current peak value and faster decay speed of pyroelectric current are observed. It is worth noting that doping via incorporating electron donor or acceptor species into the host crystal can be employed to tune the pyroelectric and thermal properties of semiconductors,[29,58] such as p, H, and G_T. These parameters also have remarkable influences on the generation and decay of instantaneous pyroelectric current (charge), and further influence the pyro-phototronic effect.

Finally yet importantly, the photoresponse of PDs as functions of chopping frequency is shown in Figure S19 (Supporting Information). With increasing the chopper frequency, the amount of pyropolarization charges will increase, which is induced by a larger temperature gradient $\mathrm{d}T/\mathrm{d}t$. Increasing the chopper frequency in low frequency range, the pyro-photocurrent of the PD increases accordingly. As the chopper frequency exceeded certain value, the variation of pyro-photocurrent of the PD witnessed a downward trend. The phenomena can be attributed to low resonance frequency of the as-prepared devices in the circuit.[59] Another five-pair self-powered PDs were constructed and checked (Figure S20, Supporting Information). It is confirmed that the incorporation of Ga dopant in ZnO MWs can significantly influence the photodetecting performances and pyro-phototronic effect undoubtedly.

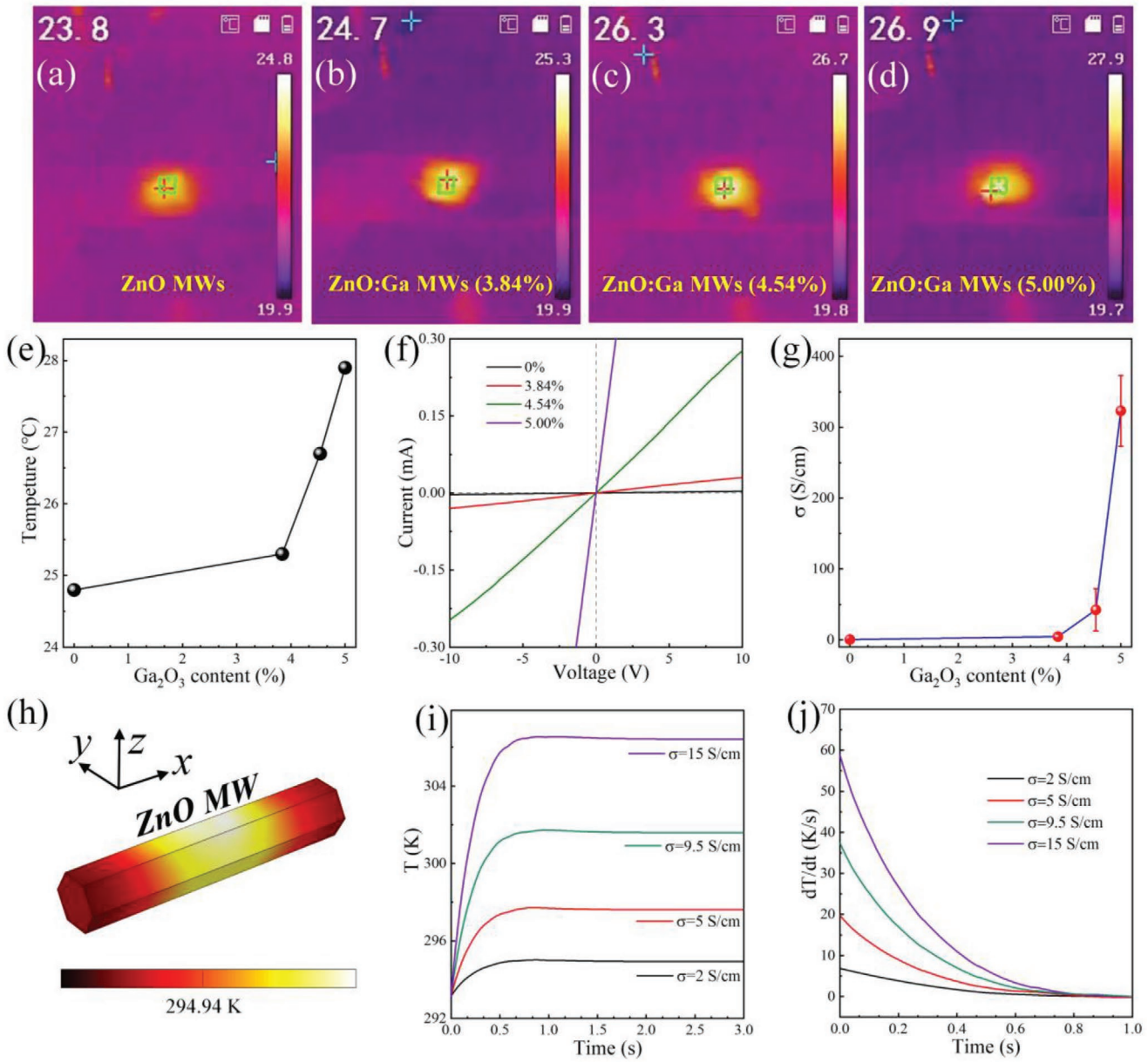

Figure 5. Thermal imaging of a) undoped ZnO MWs, b) ZnO:Ga MWs (3.84%), c) ZnO:Ga MWs (4.54%), d) ZnO:Ga MWs (5.00%) under UV illumination (370 nm, 10.0 mW cm^{-2}). The corresponding temperature ranges are shown in right. e) Maximum temperature with respect to the Ga doping concentration. f) *I*–*t* curves of ZnO:Ga MWs by varying Ga concentrations. g) The calculated electrical conductivity of individual ZnO:Ga MWs with respect to various Ga concentrations. h) The distribution of simulated surface temperature of a ZnO MW under UV illumination (370 nm, 10.0 mW cm^{-2}). i) The simulated temperature *T* and j) temperature variation rate d*T*/d*t* of the single MW with different electrical conductivities (σ) as functions of time.

3. Conclusion

In summary, a self-powered PD based on single ZnO:Ga MW/p$^+$-GaN heterojunction is constructed with the performances enhanced by pyro-phototronic effect. By varying the concentration of Ga dopant, the coupling process of pyroelectric and photovoltaic effects can be tuned to further optimize the device performances. It is illustrated that the Ga doping not only influences photovoltaic current through the formed n-ZnO:Ga/p$^+$-GaN heterojunction, but also provides an alternate approach to increase the pyroelectric current by mediating more heat. The enhanced pyroelectric responsivity (detectivity) can be utilized to compensate the decreased photovoltaic responsivity (detectivity) in highly doped ZnO:Ga MW PDs, breaking the doping limitation of the as-constructed n-ZnO:Ga MW/p$^+$-GaN heterojunction photodetection devices. Moreover, the decay time of pyroelectric current shortens due to the rapid disappearance of temperature change with an increase of the Ga doping concentration. These findings are used to study coupling mechanism of integrating pyroelectric and photovoltaic effects modulated by doping concentration, which provides a theoretical and experimental basis for developing

high-performance self-powered photodetectors based on pyro-phototronic effect.

4. Experimental Section

Device Fabrication: The undoped ZnO MWs and Ga-doped ZnO (ZnO:Ga) MWs employed in this work were synthesized via CVD method as reported in the previous literature.[35,60] For the case of ZnO:Ga MWs with different Ga doping concentration, ZnO power (99.99% purity), Ga_2O_3 power (99.999% purity), and graphite (C) powder (99.999% purity) with the weight ratio, such as 12:1:13, 10:1:11, and 9:1:10, were mixed thoroughly and used as the precursors. Increasing the weight ratio of Ga_2O_3 powder in the mixed precursors can be employed to tune the Ga doping concentration in the as-synthesized samples.[35,50,60] The corresponding synthesized MWs are denoted nominally as ZnO:Ga MW (3.84 wt%), ZnO:Ga MW (4.54 wt%), and ZnO:Ga MW (5.00 wt%), respectively.[61] A single MW based heterojunction photodetector made of a MW and p^+-GaN substrate was constructed. First, MgO nanofilm working as an insulating layer, was evaporated on the pre-cleaned p^+-GaN substrate with Mg-doping concentration of 1×10^{20} cm^{-3} by using molecular beam epitaxy system. Ni/Au (30/30 nm) electrodes were deposited on p^+-GaN substrate using the electron beam evaporation system and subsequently followed by annealing. Next, a single MW was picked out and then transferred across the boundary between the MgO insulating layer and the p^+-GaN substrate. Finally, indium (In) particle was applied on the MW to act as the electrode. A n-p^+ heterojunction architecture (n-ZnO MW/p^+-GaN) was formed.

Device Characterization: The morphology characteristics of the as-prepared MWs were checked by using scanning electron microscope (SEM). The crystallographic property of the MWs was characterized by using X-ray diffraction (XRD). The optical property of MWs was measured by photoluminescence (PL) spectrometer with a He–Cd laser acting as the excitation source at the wavelength of 325 nm. Absorption spectra of MWs were measured by using ultraviolet–infrared (UV–NIR) microabsorption spectrum system (MStarter ABS). The photoelectric performance of the as-constructed single MW/p^+-GaN heterojunction PD was measured by a detecting system consisting of a Xe lamp, monochromator, chopper, and semiconductor analysis device (Keithley B1500A). The intensity of incident light was measured using a digital power meter (Vega, Ophir) with a thermal sensor (3A, Ophir). A heating platform (JF966-1015) was employed for the adjustment of ambient temperature.

Supporting Information

Supporting Information is available from the Wiley Online Library or from the author.

Acknowledgements

This work was supported by the National Natural Science Foundation of China (Grant Nos. 11974182, 11774171, 21805137, and 11874220), the Fundamental Research Funds for the Central Universities (Grant No. NT2020019), Open Fund of Key Laboratory for Intelligent Nano Materials and Devices of the Ministry of Education (Grant No. INMD-2020M03).

Conflict of Interest

The authors declare no conflict of interest.

Data Availability Statement

Research data are not shared.

Keywords

coupling mechanism, doping concentration, pyro-phototronic effect, self-powered photodetectors

Received: August 31, 2021
Revised: October 22, 2021
Published online: November 23, 2021

[1] W. Tian, Y. Wang, L. Chen, L. Li, *Small* **2017**, *13*, 1701848.
[2] H. Chen, P. Yu, Z. Zhang, F. Teng, L. Zheng, K. Hu, X. S. Fang, *Small* **2016**, *12*, 5809.
[3] Y. Zhang, W. Xu, X. Xu, J. Cai, W. Yang, X. S. Fang, *J. Phys. Chem. Lett.* **2019**, *10*, 836.
[4] R. Zhuo, L. Zeng, H. Yuan, D. Wu, Y. Wang, Z. Shi, T. Xu, Y. Tian, X. Li, Y. H. Tsang, *Nano Res.* **2019**, *12*, 183.
[5] W. D. Song, J. X. Chen, Z. L. Li, X. S. Fang, *Adv. Mater.* **2021**, *33*, 2101059.
[6] N. Ma, Y. Yang, *Nano Energy* **2017**, *40*, 352.
[7] D. Wu, Z. Zhao, W. Lu, L. Rogée, L. Zeng, P. Lin, Z. Shi, Y. Tian, X. Li, Y. H. Tsang, *Nano Res.* **2021**, *14*, 1973.
[8] F. Teng, W. Ouyang, Y. Li, L. Zheng, X. S. Fang, *Small* **2017**, *13*, 1700156.
[9] X. Wang, Y. Dai, R. Liu, X. He, S. Li, Z. L. Wang, *ACS Nano* **2017**, *11*, 8339.
[10] Y. Yang, W. Guo, K. Pradel, G. Zhu, Y. Zhou, Y. Zhang, Y. Hu, L. Lin, Z. Wang, *Nano Lett.* **2012**, *12*, 2833.
[11] Z. Wang, R. Yu, C. Pan, Z. Li, J. Yang, F. Yi, Z. L. Wang, *Nat. Commun.* **2015**, *6*, 8401.
[12] W. Peng, R. Yu, X. Wang, Z. Wang, H. Zou, Y. He, Z. L. Wang, *Nano Res.* **2016**, *9*, 3695.
[13] G. Heiland, H. Ibach, *Solid State Commun.* **1966**, *4*, 353.
[14] D. You, C. Xu, W. Zhang, J. Zhao, F. Qin, Z. Shi, *Nano Energy* **2019**, *62*, 310.
[15] C. C. Hsiao, K. Y. Huang, Y. C. Hu, *Sensors* **2008**, *8*, 185.
[16] M. Kumar, M. Patel, T. T. Nguyen, J. Kim, J. Yi, *Nanoscale* **2018**, *10*, 6928.
[17] A. K. Rana, M. Kumar, D. K. Ban, C. P. Wong, J. Yi, J. Kim, *Adv. Electron. Mater.* **2019**, *5*, 1900438.
[18] Y. Wang, L. Zhu, Y. Feng, Z. Wang, Z. L. Wang, *Adv. Funct. Mater.* **2019**, *29*, 1807111.
[19] W. Peng, X. Wang, R. Yu, Y. Dai, H. Zou, A. C. Wang, Y. He, Z. L. Wang, *Adv. Mater.* **2017**, *29*, 1606698.
[20] Z. Song, H. Zhou, C. Ye, L. Yang, M. Xue, J. Mei, H. Wang, *Mater. Sci. Semicond. Process.* **2017**, *64*, 101.
[21] B. D. Boruah, *Nanoscale Adv.* **2019**, *1*, 2059.
[22] Z. Wang, R. Yu, X. Wang, W. Wu, Z. L. Wang, *Adv. Mater.* **2016**, *28*, 6880.
[23] Z. Xu, Y. Zhang, Z. Wang, *J. Phys. D: Appl. Phys.* **2019**, *52*, 223001.
[24] Y. Zhu, B. Wang, C. Deng, Y. Wang, X. Wang, *Nano Energy* **2021**, *83*, 105801.
[25] Y. Ning, Z. Zhang, F. Teng, X. S. Fang, *Small* **2018**, *14*, 1703754.
[26] C. Y. Tsay, I. P. Hsiao, F. Y. Chang, C. L. Hsu, *Mater. Sci. Semicond. Process.* **2021**, *121*, 105295.
[27] R. Saha, A. Karmakar, S. Chattopadhyay, *Opt. Mater.* **2020**, *105*, 109928.
[28] B. D. Boruah, S. N. Majji, S. Nandi, A. Misra, *Nanoscale* **2018**, *10*, 3451.
[29] S. K. Saha, M. A. Rahman, M. R. H. Sarkar, M. Shahjahan, M. K. R. Khan, *J. Semicond.* **2015**, *36*, 033004.
[30] D. K. Macharia, S. Sarker, B. Zhu, Y. Zhang, Z. Liu, N. Yu, Z. Chen, *Chem. Eng. J.* **2021**, *425*, 130638.

[31] L. Trinca, A. Galca, A. Boni, M. Botea, L. Pintilie, *Appl. Surf. Sci.* **2018**, *427*, 29.
[32] H. Wang, H. Chen, L. Li, Y. Wang, L. Su, W. Bian, B. Li, X. S. Fang, *J. Phys. Chem. Lett.* **2019**, *10*, 6850.
[33] R. Zhuo, Y. Wang, D. Wu, Z. Lou, Z. Shi, T. Xu, J. Xu, Y. Tian, X. Li, *J. Mater. Chem. C* **2018**, *6*, 299.
[34] M. Kumar, M. Patel, J. Kim, D. Lim, *Nanoscale* **2017**, *9*, 19201.
[35] H. Zou, G. Dai, A. C. Wang, X. Li, S. L. Zhang, W. Ding, L. Zhang, Y. Zhang, Z. L. Wang, *Adv. Mater.* **2020**, *32*, 1907249.
[36] G. C. Park, S. M. Hwang, J. H. Lim, J. Joo, *Nanoscale* **2014**, *6*, 1840.
[37] V. Krishnamurthi, T. Ahmed, M. Mohiuddin, A. Zavabeti, N. Pillai, C. F. McConville, N. Mahmood, S. Walia, *Adv. Opt. Mater.* **2021**, *9*, 2100449.
[38] M. S. Kim, K. G. Yim, J. S. Son, J. Y. Leem, *Bull. Korean Chem. Soc.* **2012**, *33*, 1235.
[39] T. Gao, Q. Zhang, J. Chen, X. Xiong, T. Zhai, *Adv. Opt. Mater.* **2017**, *5*, 1700206.
[40] L. Zhang, P. Wan, T. Xu, C. Kan, M. Jiang, *Opt. Express* **2021**, *29*, 19202.
[41] Y. Liu, M. Jiang, Z. Zhang, B. Li, H. Zhao, C. Shan, D. Shen, *Nanoscale* **2018**, *10*, 5678.
[42] W. Mao, M. Jiang, J. Ji, Y. Liu, C. Kan, *Opt. Express* **2019**, *27*, 33298.
[43] S. B. Lang, *Phys. Today* **2005**, *58*, 31.
[44] M. C. Larciprete, M. Centini, *Appl. Phys. Rev.* **2015**, *2*, 031302.
[45] M. Dai, H. Chen, R. Feng, W. Feng, Y. Hu, H. Yang, G. Liu, X. Chen, J. Zhang, C. Y. Xu, P. Hu, *ACS Nano* **2018**, *12*, 8739.
[46] M.-L. Ren, R. Agarwal, W. Liu, R. Agarwal, *Nano Lett.* **2015**, *15*, 7341.
[47] X. Han, K. Wang, H. Long, H. Hu, J. Chen, B. Wang, P. Lu, *ACS Photonics* **2016**, *3*, 1308.
[48] C. Bowen, J. Taylor, E. LeBoulbar, D. Zabek, A. Chauhan, R. Vaish, *Energy Environ. Sci.* **2014**, *7*, 3836.
[49] H. You, Y. Jia, Z. Wu, F. Wang, H. Huang, Y. Wang, *Nat. Commun.* **2018**, *9*, 2889.
[50] K. Y. Lo, Y. J. Huang, J. Y. Huang, Z. C. Feng, W. E. Fenwick, M. Pan, I. T. Ferguson, *Appl. Phys. Lett.* **2007**, *90*, 161904.
[51] P. Wan, M. Jiang, T. Xu, Y. Liu, C. Kan, *J. Mater. Sci. Technol.* **2021**, *93*, 33.
[52] H. Zhou, L. Yang, P. Gui, C. R. Grice, Z. Song, H. Wang, G. Fang, *Sol. Energy Mater. Sol. Cells* **2019**, *193*, 246.
[53] D. A. Neamen, *Semiconductor Physics and Devices: Basic Principles*, 3rd ed., Irwin Inc., Boston, MA **1992**.
[54] B. Saleh, M. Teich, *Fundamentals of Photonics*, 2nd ed., Wiley, New York **2007**.
[55] Y. Sun, X. Yan, X. Zheng, Y. Li, Y. Liu, Y. Shen, Y. Ding, Y. Zhang, *Nano Res.* **2017**, *10*, 77.
[56] O. Synhaivskyi, D. Albertini, P. Gaffuri, J. M. Chauveau, V. Consonni, B. Gautier, G. Bremond, *J. Phys. Chem. C* **2021**, *125*, 15373.
[57] M. R. Hossan, P. Dutta, *Int. J. Heat Mass Transfer* **2012**, *55*, 3412.
[58] S. Shinde, P. Shinde, Y. Oh, D. Haranath, C. Bhosale, K. Rajpure, *Appl. Surf. Sci.* **2012**, *258*, 9969.
[59] Y. Feng, Y. Zhang, Y. Wang, Z. L. Wang, *Nano Energy* **2018**, *54*, 429.
[60] M. Jiang, G. He, H. Chen, Z. Zhang, L. Zheng, C. Shan, D. Shen, X. S. Fang, *Small* **2017**, *13*, 1604034.
[61] G. D. Yuan, W. J. Zhang, J. S. Jie, X. Fan, J. X. Tang, I. Shafiq, Z. Z. Ye, C. S. Lee, S. T. Lee, *Adv. Mater.* **2008**, *20*, 168.